Soft Matter

Clustering and phase separation in mixtures of dipolar and active particles

Journal:	*Soft Matter*
Manuscript ID	SM-ART-11-2019-002311.R1
Article Type:	Paper
Date Submitted by the Author:	13-Mar-2020
Complete List of Authors:	Maloney, Ryan; North Carolina State University, Chemical and Biomolecular Engineering Liao, Guo-Jun; Technische Universitat Berlin, Institute of Theoretical Physics, Sec. EW 7-1 Klapp, Sabine; Technische Universitat Berlin, Institute of Theoretical Physics Hall, Carol; North Carolina State University, Chemical and Bimolecular Engineering

SCHOLARONE™
Manuscripts

Please do not adjust margins

ARTICLE

Clustering and phase separation in mixtures of dipolar and active particles

Received 00th January 20xx,
Accepted 00th January 20xx

DOI: 10.1039/x0xx00000x

Ryan C. Maloney,[a] Guo-Jun Liao,[b] Sabine H. L. Klapp[b] and Carol K. Hall*[a]

The self-assembly of colloidal particles in dynamic environments has become an important field of study because of potential applications in fabricating out-of-equilibrium materials. We investigate the phase behavior of mixtures of passive dipolar colloids and active soft spheres using Brownian dynamics simulations in two dimensions. The phase behaviors exhibited include dipolar percolated network, dipolar string-fluid, isotropic fluid, and a phase-separated state. We find that the clustering of dipolar colloids is enhanced in the presence of slow-moving active particles compared to the clustering of dipolar particles mixed with passive particles. When the active particle motility is high, the chains of dipolar particles are either broken into short chains or pushed into dense clusters. Motility-induced phase separation into dense and dilute phases is also present. The area fraction of particles in the dilute phase increases as the fraction of active particles in the system decreases, while the area fraction of particles in the dense phase remains constant. Our findings are relevant to the development of reconfigurable self-assembled materials.

1 Introduction

The collective behavior of self-propelled (active) matter – materials that convert energy from an internal or external source into translational or rotational motion[1,2] – is of interest across a broad range of sciences. From a biological perspective, the study of active matter aids in the understanding of the movement of bacteria colonies,[3,4] fish schools,[5,6] bird flocks,[7] and even pedestrian traffic.[8-10] From a fundamental physics perspective, the study of active matter has yielded insights into phase separation dynamics,[11-13] meso-scale turbulence,[14-16] swarming,[17-20] swirling,[21] and laning.[22,23] Computer-simulated and artificial active colloidal particles are an ideal model system for studying the collective behavior of active matter because we have greater control over the interactions between constituent particles in these systems than we do over interactions in biological systems.[24-31] Mixtures of active and passive particles, in particular, display interesting collective behavior including active-passive segregation,[32-34] flocking,[35] and facilitation of attraction-induced phase separation.[36]

Perhaps the most well studied model for simulating systems of active particles is the active Brownian particle (ABP) model.[37,38] The traditional ABP model consists of spheres that experience self-propulsive forces, Brownian motion, and short-range interparticle repulsive forces, but neglects other interactions such as phoretic and hydrodynamic forces.[39] Despite these simplifications, the ABP model offers insight into the interplay between activity, random motion, and excluded volume interactions. The traditional ABP model has been used to characterize motility-induced phase separation (MIPS),[11,31,39-41] in which a sufficiently dense system of ABPs undergoes a transition from a homogeneous isotopic fluid at low Péclet number to a large dense cluster in coexistence with a dilute gas-like phase at high Péclet number. Motility-induced phase separation is analogous to the equilibrium liquid-gas phase separation exhibited by passive particles with attractive interactions; however, MIPS occurs even in the absence of attractive interactions in the ABP model which contains only repulsive interactions. The observation of MIPS in the absence of attractive interactions, which normally drive phase separation, is instead explained through either a kinetic theory or continuum mean-field theory. The kinetic theory of MIPS posits that clusters arise via a self-trapping mechanism.[42,43] In this explanation, a pair of colliding particles remain in contact until rotational diffusion leads them to orient away from one another, allowing them to move apart. If additional particles collide with the pair during the reorientation time, the cluster will grow. Continuum mean-field theory for MIPS explains phase separation as resulting from a reduction in the particle effective speed due to an increase in local density.[12,44,45] An attractive feature of the ABP model is that it readily lends itself to the investigation of more complex systems such as rod-shaped particles,[46,47] hydrodynamically-interacting particles,[48-50] particles with short-range attractive interactions,[51] anisotropic interactions,[52,53] and eccentric (or circle) swimmers.[54]

---

[a] *Department of Chemical & Biomolecular Engineering, North Carolina State University, Raleigh, NC 27695, USA. E-mail: hall@ncsu.edu*

[b] *Institut für Theoretische Physik, Technische Universität Berlin, Hardenbergstr. 36, D10623 Berlin, Germany.*

Please do not adjust margins

Mixtures of active and passive particles is of particular interest given that real world systems often contain one or more active components. Some examples of such systems are swimming bacteria moving around nutrient granules,[55] dynamic processes within cells,[56] and predator-prey behavior.[57,58] Many of the colloidal mixtures with active components that have been reported thus far involve a small number of active components, such as the so called "tracer particle" experiments in which a single passive particle is placed in an active medium,[59-63] or active dopant experiments in which a small number particles drive crystallization of passive particles.[64] There have also been investigations into the effects of an active bath on a small number of passive particles.[65] Recently there has been a shift to investigating systems where the number of constituent particles is more equitable. These include simulations of active and passive repulsive spheres,[33,66-70] mixtures of active particles with different motilities,[32,71] and mixtures of chiral (clockwise and counter clockwise circle swimmers) active particles.[34] We add to this body of work by characterizing the phase behavior of a mixture consisting of passive dipolar spheres and ABPs.

Colloidal particles with induced or permanent dipoles exhibit complex behavior due to the anisotropic and long-ranged nature of dipole-dipole interactions. A polarizable colloidal particle placed in an AC field will experience an internal charge separation in the direction of the field, effectively creating an induced dipole in the particle. Application of a homogenous field in one direction will cause particles with induced dipoles to assemble into chains. This has been used to assemble flexible nano- and micro- wires and chains,[72,73] crystals,[74] and other responsive materials.[75,76] Colloidal particles with permanent dipoles have also been extensively studied by simulations[77-79] Such particles form rings, small chains, gels, and branched networks at low and intermediate density, and crystalline phases at high density. While we focus on the behavior of passive dipolar particles, we note that there has recently been interest in active dipolar particles,[53,80-83] including studies that characterize the behavior of magnetotatic bacteria that move with or against the earth's magnetic field.[84-87]

In this paper, we present results from Brownian dynamics simulations of two-dimensional mixtures of passive dipolar spheres and active repulsive particles. We explore how the interplay between particle area fraction, the fraction of total particles that are active colloids, and the active particle Péclet number affects the phases formed by the mixture and the local structure of those phases. We have simulated systems with low and intermediate area fractions between 0.05 and 0.55, but do not consider high area fraction systems where crystalline phases would be expected. The active particle fractions considered are 0.2, 0.4, 0.6, and 0.8. In addition, we simulate all-active and all-dipole systems to serve as a point of comparison for our mixtures. We compute the extent of polymerization and the percolation probability to characterize the behavior of the dipolar particles. In addition, we measure the largest cluster size for dipolar colloids, active colloids, and both colloids combined. Finally, we take local area fraction measurements to determine the conditions under which phase separation is present.

Highlights of our results include the following. Phase diagrams at constant area fraction were calculated in the active particle fraction-Péclet number plane. The mixtures form percolated networks of dipolar colloids, dipolar string-fluids, and isotropic fluids; they can also phase separate into a dense and a dilute phase, depending on the area fraction of the system, the ratio between the number of active and dipolar particles, and the Péclet number of the active particles. The mixtures display an interesting interplay between the two types of particles in which the dipolar colloids tend to form chains or clusters and the active particles either assist or hinder the formation of these supracolloidal structures. At low active particle Péclet number, the phases formed are similar to those formed in single component dipolar systems, with the active particles pushing dipolar particles together. At high Péclet number, the phases formed are similar to those formed by single-component active systems, but the distribution of the two species of particles between the two phases is unequal.

2 Model and methods of investigation

2.1 Model system

We perform Brownian dynamics simulations in two dimensions (2D) on a binary mixture of colloidal particles. Particles in the mixture are either passive dipolar soft-spheres or active soft-spheres. The motion of particle i with position $\boldsymbol{r}_i$ and orientation $\boldsymbol{u}_i$ is calculated by solving the coupled overdamped Langevin equations:[88,89]

$$\dot{\boldsymbol{r}}_i(t) = \beta D_t\left[f_i \cdot \boldsymbol{u}_i(t) + \boldsymbol{F}_i\right] + \sqrt{2D_t}\boldsymbol{\xi}_i(t),1$$

$$\dot{\boldsymbol{u}}_i(t) = \left[\beta D_r \boldsymbol{T}_i + \sqrt{2D_r}\boldsymbol{\Gamma}_i(t)\right] \times \boldsymbol{u}_i(t).2$$

In equation 1 and 2, $\dot{\boldsymbol{r}}$ and $\dot{\boldsymbol{u}}$ are the time (t) derivatives of the position and orientation of particle i respectively, $\boldsymbol{F}_i$ and $\boldsymbol{T}_i$ are the forces and torques acting on particle i respectively, D_t is the translational diffusion constant, and D_r is the rotational diffusion constant. The thermal energy is $\beta = 1/k_BT$ (with k_B as Boltzmann's constant and T as temperature), and f_i is a constant self-propulsive force for the active particles. For passive particles, such as the dipolar colloids in our mixtures, $f_i = 0$. Translational $(\boldsymbol{\xi}_i(\mathrm{t}))$ and rotational $(\boldsymbol{\Gamma}_i(\mathrm{t}))$ thermal noise terms represent random collisions between the colloidal particles and solvent. These are Gaussian white noise terms that fulfill the relations $\langle \boldsymbol{\xi}_i(\mathrm{t})\rangle = \langle \boldsymbol{\Gamma}_i(\mathrm{t})\rangle = 0$, $\langle \xi_{i,v}(t)\xi_{j,w}(t')\rangle = 2\delta_{ij}\delta_{vw}\delta(t-t')/(\mathrm{D}_t\beta^2)$, and $\langle \Gamma_{i,v}(t)\Gamma_{j,w}(t')\rangle = 2\delta_{ij}\delta_{vw}\delta(t-t')/(\mathrm{D}_r\beta^2)$, where δ_{mn} is the Kronecker delta, the angle brackets denote ensemble average, and $\xi_{i,v}(t)$ and $\Gamma_{i,v}(t)$ denote the v (x or y) component of $\boldsymbol{\xi}_i(t)$ and $\Gamma_i(t)$ for the ith particle, respectively.

The forces $(\boldsymbol{F}_i)$ and torques $(\boldsymbol{T}_i)$ acting on particle i are computed as

$$\boldsymbol{F}_i = -\nabla_{\boldsymbol{r}_i}U,3$$

Please do not adjust margins

Please do not adjust margins

$$\boldsymbol{T}_i = -\boldsymbol{u}_i \times \nabla_{\boldsymbol{u}_i} U . 4$$

In equations 3 and 4, U is the total potential energy of the system, which is the sum of all inter-particle pairwise interactions. Particles interact via a combination of the Weeks-Chandler-Anderson (WCA) potential[88] and the dipole-dipole potential. The WCA potential (U_{WCA}) accounts for steric repulsion between all colloids, and the dipole-dipole potential (U_D) accounts for dipolar interactions between pairs of dipolar colloids. The equations for U_{WCA} and U_D are

$$U_{WCA}(r_{ij}) = \begin{cases} 4\varepsilon\left[\left(\frac{\sigma}{r_{ij}}\right)^{12} - \left(\frac{\sigma}{r_{ij}}\right)^{6} + \frac{1}{4}\right], & r_{ij} < 2^{1/6}\sigma \\ 0 & , \; r_{ij} \geq 2^{1/6}\sigma \end{cases} , 5$$

$$U_D(\boldsymbol{r}_{ij}, \boldsymbol{\mu}_i, \boldsymbol{\mu}_j) = \frac{\boldsymbol{\mu}_i \cdot \boldsymbol{\mu}_j}{r_{ij}^3} - 3\frac{(\boldsymbol{\mu}_i \cdot \boldsymbol{r}_{ij})(\boldsymbol{\mu}_j \cdot \boldsymbol{r}_{ij})}{r_{ij}^5} , 6$$

where σ is the unit of length, r_{ij} is the distance between particle i and particle j, $\boldsymbol{r}_{ij} = \boldsymbol{r}_j - \boldsymbol{r}_i$ is the vector connecting the center of the two particles, and $\boldsymbol{\mu}_i$ is the dipole moment of particle i. We set the repulsive strength $\varepsilon^* = \beta\varepsilon = 100$ to minimize particle overlap. We fix the dipole moment to the particle orientation, so $\boldsymbol{\mu}_i = \mu \boldsymbol{u}_i$ where μ is the magnitude of the dipole moment. Ewald summation is used to account for the long-range nature of the dipole-dipole potential.[91-94] We use Ewald summation over other techniques such as a shifted force potential because some of our mixtures contain a small number of dipolar particles, which would result in finite size effects had we used a truncation method.[95] For a description of the Ewald summation equations used, please refer to the Appendix of Ref. 53. The values for the Ewald summation parameters we use (convergence parameter $\alpha = 7/L$, truncation wave number $m = 15$, and cut-off radius for the real part of the dipolar interactions $r_c = L/2$, with L as the box length) match those used in a similar system of active dipolar particles.[53] All simulations were performed with a coupling strength $\lambda = \beta\mu^2/\sigma^3 = 10$ between dipoles to ensure strongly coupled dipolar colloids.

The rotational diffusion coefficient D_r and translation diffusion coefficient D_t are related via the Stokes-Einstein relationship which says that $D_r = 3D_t/\sigma_h^2$ for a hard sphere with particle diameter σ_h. Since the particles in our model are soft-spheres, we define an effective hard-sphere diameter in terms of the unit of length σ from equation 5 as described by Liao and Klapp,[54] following the work of Barker and Henderson[96] via $\sigma_h = \int_0^\infty (1 - \exp[-\beta U_{WCA}(r)])dr$. With our choice of $\varepsilon^* = 100$, the resulting effective hard-sphere diameter is $\sigma_h \approx 2^{1/6}\sigma$. Substituting this result into the Stokes-Einstein relationship, we obtain $D_r = 3 \times 2^{-1/3} D_t/\sigma^2$.

2.2 Simulation Parameters

Simulations are performed on $N = 2000$ total colloids in an $L \times L$ square box with periodic boundary conditions. There are N_D dipolar colloids and N_A active colloids for a total number of colloids $N = N_D + N_A$. The fraction of particles that are active is $x_A = N_A/N$. The area fraction of the box occupied by colloids is $\Phi = N\pi\sigma^2/4L^2$. Simulations consist of at least 1.5×10^6 time steps with the maximum time between each step of $\Delta t = 5 \times 10^{-5}\tau$, where $\tau = \sigma^2/D_t$ is the unit of time. This resulted in simulations that are at least of time 75τ. Simulation "snapshots" containing particle position and orientation data are collected every 0.01τ, and data over the last 25τ of each simulation is analyzed to obtain steady-state results. Results are presented in non-dimensionalized units, where an active particle with self-propulsive force f_i has a Péclet number of $Pe = \beta\sigma f_i$.

To ensure that our simulations achieved a non-equilibrium-steady state, we calculated the average cluster sizes of dipolar particles, of active particles, and of all particles. The system was said to be in a steady-state when these values plateaued over time, which for most systems required between 25τ and 50τ. Simulations at low density with a low fraction of active particles and low Peclet number required at least 75τ to achieve steady-state, therefore these simulations were run for 100τ or longer. The simulations discussed in this work were started from randomized particle positions and orientations, which allowed the system to achieve a steady-state rapidly. Additional simulations were performed starting from fully segregated initial configurations to determine the effects of the initial configuration. Most of these segregated systems achieved a steady-state that was largely identical with that achieved from the random initial configuration, though these required longer simulation times. The exception to this was systems where the Péclet number of the active particles was zero (a fully passive system), or very low. In this case the dipolar particles formed denser clusters then the corresponding system starting from a random configuration. A full analysis of this behavior was beyond the scope of this work.

2.3 Data Analysis Parameters

In this section we describe the analysis techniques that we use to characterize the mixtures. We use subscript "D" to denote quantities that are associated only with dipolar colloids, and subscript "A" to denote quantities that are associated only with active colloids. No subscript is used for quantities associated with all of the colloids in the system regardless of type. At the end of this section we introduce the parameters used to describe the phases present in the mixtures based on these analyses.

2.3.1 Clustering behavior

The clustering behavior of both passive dipolar systems and active repulsive sphere systems is well established. Equation 6 tells us that two particles will have a minimum energy of $U_D = -2\mu^2\sigma^{-3}$ when they are separated by a distance of σ and aligned in a head-to-tail configuration. This energetically favorable configuration drives the dipolar particles to form chains. We refer our readers to the introduction for explanations of the mechanisms that lead to phase separation in ABPs and here we add that the critical density below which phase separation will not occur, Φ_{crit}, has been reported to be

Please do not adjust margins

a range of values depending on the system size and persistence length ℓ_p.[97-99] The persistence length is the distance over which an active particle retains information about its initial orientation, and is related to the particle velocity v_o and rotational diffusion constant via $\ell_p = v_o/D_R$. For two dimensions and in the ballistic regime $(D_R \to 0,\ \ell_p \gg \sigma)$, the lower limit for the critical density has been reported as $\Phi_{crit} \approx 0.28$.[100] When the rotational diffusion constant increases, the persistence length decreases and clusters break apart more rapidly, causing the value of Φ_{crit} to rise. When the translational diffusion coefficient is zero and rotational diffusion is the only source of noise, $\Phi_{crit} \approx 0.4$.[101] Based on this, we predict that the critical density for phase separation in our simulations will be $0.28 \lesssim \Phi_{crit} \lesssim 0.40$.

To quantify clustering in our systems, we use two criteria to determine if a pair of colloids are clustered with each other. First, if colloids i and j are both active soft spheres or if one is an active soft sphere and the other is a dipolar soft sphere, then they will be in a cluster if $r_{ij} < 2^{1/6}\sigma$. This criterion corresponds to colloids that are within the repulsive part of the WCA potential. Second, if both colloids i and j are dipolar soft spheres, then the colloids will be in a cluster if $r_{ij} < 1.5\sigma$ and $\boldsymbol{U}_D < 0$.[102] The distance $r_{ij} = 1.5\sigma$ is the average position of the first minimum in the radial distribution function, $g(r)$, which was found by performing simulations containing only dipolar colloids over many area fractions. The position of the first minimum of $g(r)$ has been found to be relatively insensitive to changes in temperature or density.[102] The internal energy criterion ensures that only attractive configurations are considered for clustering. A cluster is defined to be the set of colloids in which each individual particle satisfies the above criteria with at least one other colloid in that cluster; n will refer to the total number of colloids in the cluster. If a colloid does not meet these criteria with any of the other colloids in the system, then that colloid forms its own cluster of size one.

We calculate the ensemble average largest cluster size $\langle n^{lc} \rangle$ to gain an overall picture of the clustering behavior of the mixtures. We defined the fraction of colloids in the largest cluster as $\langle n^{lc} \rangle/N$. Small values of this fraction indicate that a state without any large clusters is present. Large values of $\langle n^{lc} \rangle/N$ indicate a state where many particles in the system have come together in a large cluster. When this value equals one, all particles have been incorporated in a single cluster.

The extent of polymerization E_D^{poly} is useful for characterizing the behavior of the dipolar colloids at low area fractions. The extent of polymerization is the fraction of dipolar particles that are in clusters, and is defined as $\langle N_D^{poly}(t) \rangle / N_D$, where $N_D^{poly}(t)$ is the total number of dipolar colloids that are in a cluster of at least three particles at time t. An extent of polymerization at or near 1 means that all, or nearly all, of the dipolar particles exist in clusters, while an extent of polymerization near zero means that few dipolar clusters are present. The extent of polymerization cannot distinguish between a state that contains many intermediate size clusters and one that contains one large cluster.

We use percolation probability to measure the formation of networks by the dipolar colloids in the mixtures. A percolated network is a cluster that spans the simulation box and connects back to itself.[103] This definition of percolation can be broadly satisfied by clusters that either contain primarily dipolar colloids aligned in a head-to-tail orientation or contain both dipolar and active colloids in a large, dense domain. This second type of cluster is more likely to occur in a phase separated system and will be treated in a different manner as described in section 2.3.2. Here we will focus our analysis of percolated clusters on those dominated by dipolar colloids. Percolation probability is defined as $\Pi_D = \langle s(t) \rangle$, where s characterizes the state of the configuration of particles at each time t and is assigned a value of 1 if a percolated cluster exists in the system and a value of zero if no such cluster is found.

2.3.2 Phase separation

As mentioned previously, active colloids can undergo motility-induced phase separation (MIPS) resulting in a large, densely-packed cluster in equilibrium with freely moving particles. The fraction of particles in the largest cluster gives a rough estimate for determining if phase separation exists, however, more precise determination of the conditions necessary for phase separation require additional analysis methods. One well documented method is through the analysis of the local area fraction.[42] This method not only provides information on phase separation; it allows us to gain insight into the distribution of dipolar and active colloids in the dense and gas-like phases. To calculate the local area fraction, we begin by performing Voronoi tessellation on the system configuration at any time t. The simulation cell is divided into Voronoi cells such that each cell contains one colloid plus all the space in the simulation box that is closer to that colloid than to any other colloid. The area of the ith Voronoi cell is A_i, and the local area fraction of the particle in each Voronoi cell is $\phi_i^{loc} = \pi\sigma^2/(4A_i)$. After the Voronoi tessellation is completed, we need to determine if the particles have phase separated into a dense region and a dilute region.

To determine if a dense and dilute region exist in the system, we overlay a finely-spaced square grid with mesh size $\Delta L_{pm} \sim 1.0\sigma$ on the simulation cell. Each box on this grid is identified by a set of coordinates, (x,y). The position-resolved local area fraction in each grid box, $\phi^{loc}(x,y)$, is the weighted average of ϕ_i^{loc} for those Voronoi cells that lie within each box. If a system is not phase separated, the values of $\phi^{loc}(x,y)$ will be uniformly distributed through the simulation cell and the probability distribution $P\big(\phi^{loc}(x,y)\big)$ will have a single peak. If a system has phase separated, there will be a contiguous region where $\phi^{loc}(x,y)$ is high, corresponding to the dense phase, and a second contiguous region where $\phi^{loc}(x,y)$ is low, corresponding to the dilute phase. In a phase separated system, the probability distribution $P\big(\phi^{loc}(x,y)\big)$ will have two distinct peaks. As has been reported elsewhere, this method can produce broad tails in the peaks of the probability distribution due to clusters formed in the dilute phase.[48]

Therefore, the local area fraction for each grid box is averaged over a short time interval, $\Delta\tau = 0.5\tau$, to obtain the time-averaged, position-resolved local area fraction, $\overline{\phi}^{loc}(x,y)$. Once we find $\overline{\phi}^{loc}(x,y)$, we can calculate the probability distribution for the local area fraction $P(\,\overline{\phi}^{loc}(x,y))$, and recover the two distinct peaks for the phase separated states.

In addition to allowing us to determine if a system exhibits phase separation, the local area fraction gives us information about how the active and dipolar colloids are distributed between the two phases. To extract this information, we locate the interface separating the coexisting states. To find the interface, we define the parameter $\alpha(x,y)$, which quantifies the number of colloids in the neighborhood of the grid box at (x,y),

$$\alpha(x,y) \equiv (\Delta L_{pm})^2 \sum_{j,k=-1}^{1} \overline{\phi}^{loc}(x + j\Delta L_{pm}, y + k\Delta L_{pm}).$$

In the above equation, (x,y) refers to the coordinates that identify a grid box on the coarse, particle-resolved grid and the sum is over the $\overline{\phi}^{loc}(x,y)$ of the eight grid boxes surrounding that central grid box (omitting the term where $\mathrm{j} = \mathrm{k} = 0$). We calculate $\alpha(x,y)$ for each of the particle-resolved grid boxes. The interface is the set of boxes that satisfy the selection criteria $|\alpha(x,y) - \alpha_{thres}| \le \delta\alpha_{thres}$ where $\alpha_{thres} = 4.0$ and $\delta\alpha_{thres} = 0.4$. This choice means that the interfacial grid points have a time-averaged number of neighbors equal to 4; it creates an interface that matches well with the interface seen in simulation snapshots. Once the set of interfacial boxes is found, we can measure the local area fraction as a function of the distance from the interface $\phi(d)$ and fit the data with the Cahn-Hillard ansatz:[104]

$$\phi(d) = \frac{\phi_{dense} + \phi_{gas}}{2} + \frac{\phi_{dense} - \phi_{gas}}{2}\tanh\left(\frac{d - d_o}{w}\right), \#7$$

where d_o is the location of the midpoint between dense and dilute phases and w is related to the width of the interface between these regions. From this we can extract the local area fraction in the dense phase ϕ_{dense} and in the gas-like phase ϕ_{gas}.

To estimate the degree of hexagonal ordering present in the simulations we calculate the hexagonal bond-orientational order parameter.[105] The hexagonal bond-orientational order parameter for the jth particle is

$$\Psi_{j,6} = \frac{1}{N_j^{nbr}}\left|\sum_{k \in N_j^{nbr}} e^{i6\theta_{jk}}\right|,$$

where the sum is over N_j^{nbr} neighbors of the jth particle and k identifies the neighboring particle. The angle θ_{jk} is formed between the vector $\boldsymbol{r}_{jk}$ (that is, the vector connecting the center of particles j and k) and a fixed but arbitrary vector. The neighbors of a particle are defined to be the colloids that reside in the Voronoi cells adjacent to the cell that contains that particle. When $\Psi_{j,6} = 1$ for all particles, the system is in a perfect hexagonal configuration. A disordered system will have small values of $\Psi_{j,6}$ for all particles.

2.3.3 Phase definitions and criteria

Using the above analysis techniques, we can identify four different types of phase behavior that our mixtures exhibit: motility-induced phase separation (MIPS), dipolar percolation, dipolar string-fluid, and isotropic fluid. The MIPS phase has both a large dense cluster and a sparsely populated region of freely moving colloids. This phase is characterized by two distinct peaks in $P(\,\overline{\phi}^{loc}(x,y))$, as well as a clear boundary between the dense and dilute regions. The remaining three types of behavior do not exhibit phase separation. The dipolar percolation phase has a cluster of dipolar particles that spans across the periodic boundary of the simulation box and connects back to itself in at least one dimension. This phase is defined to occur when the dipolar percolation probability $\Pi_D \ge 0.75$. The dipolar string-fluid phase is one in which there is large amount of polymerization between dipolar particles, but the system neither percolates nor exhibits MIPS. This phase is defined to occur when the dipolar percolation probability $\Pi_D < 0.75$ and the extent of polymerization $\phi_D^{poly} > 0.75$. The isotropic fluid phase is one in which there is little polymerization between dipolar particles and no MIPS. This phase is defined to occur when both the percolation probability $\Pi_D < 0.75$ and the extent of polymerization $\phi_D^{poly} < 0.75$.

3. Results and Discussion

In the following sections, we present the results of our simulations of mixtures of dipolar soft spheres and active soft spheres. We first analyze clustering of the colloids, focusing our discussion on the results from simulations at $\Phi = 0.15$, which is representative of a low-density system where MIPS does not occur, and $\Phi = 0.45$, which is representative of a high-density system that does exhibit MIPS. Next, we will analyze the phase separation that occurs at $\Phi = 0.45$. Following this, we present the phase diagram in the active fraction versus Péclet number $(x_A\ vs.Pe)$ plane for constant values of the area fraction between $\Phi = 0.05$ and $\Phi = 0.55$. Finally, we discuss in more detail the underlying structure of the phases summarized in the phase diagrams.

3.1 Cluster Formation

We first turn our attention to the clustering behavior of the mixtures. Figure 1 shows the fraction of colloids of type k (where k is "D" for dipolar particles, "A" for active particles, or "All" for all particles) in the largest cluster of type k, $\langle n_k^{lc}\rangle/N_k$, versus Péclet number. Figure 1(a) shows these results for the system at area fraction $\Phi = 0.15$ and active particle fraction $x_A = 0.4$. In this figure we see that at Péclet number $Pe = 0$, the fraction of dipolar particles in the largest dipolar cluster, $\langle n_D^{lc}\rangle/N_D \approx 0.57$. When $Pe = 5$, this value increases slightly to $\langle n_D^{lc}\rangle/N_D \approx 0.6$. When Péclet number is increased above $Pe = 5$, the value of $\langle n_D^{lc}\rangle/N_D$ decreases rapidly, approaching zero. The behavior of the fraction of particles in the largest cluster of all particles, $\langle n_{All}^{lc}\rangle/N$, mirrors that seen in $\langle n_D^{lc}\rangle/N_D$.

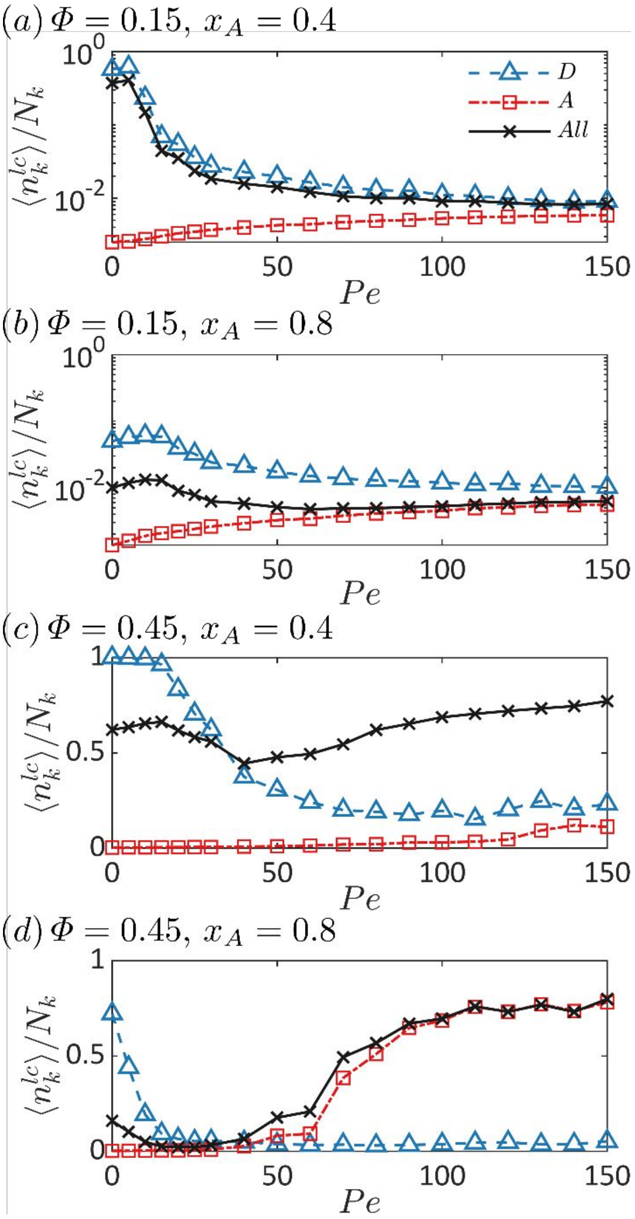

Figure 1: Fraction of particles in the largest cluster versus Péclet number for dipolar colloids (blue triangles), active colloids (red squares), and all colloids (black 'x') for (a) $\Phi = 0.15$, $x_A = 0.4$ (b) $\Phi = 0.15$, $x_A = 0.8$ (c) $\Phi = 0.45$, $x_A = 0.4$ and (d) $\Phi = 0.45$, $x_A = 0.8$. Note that (a) and (b) are plotted on a log scale for clarity.

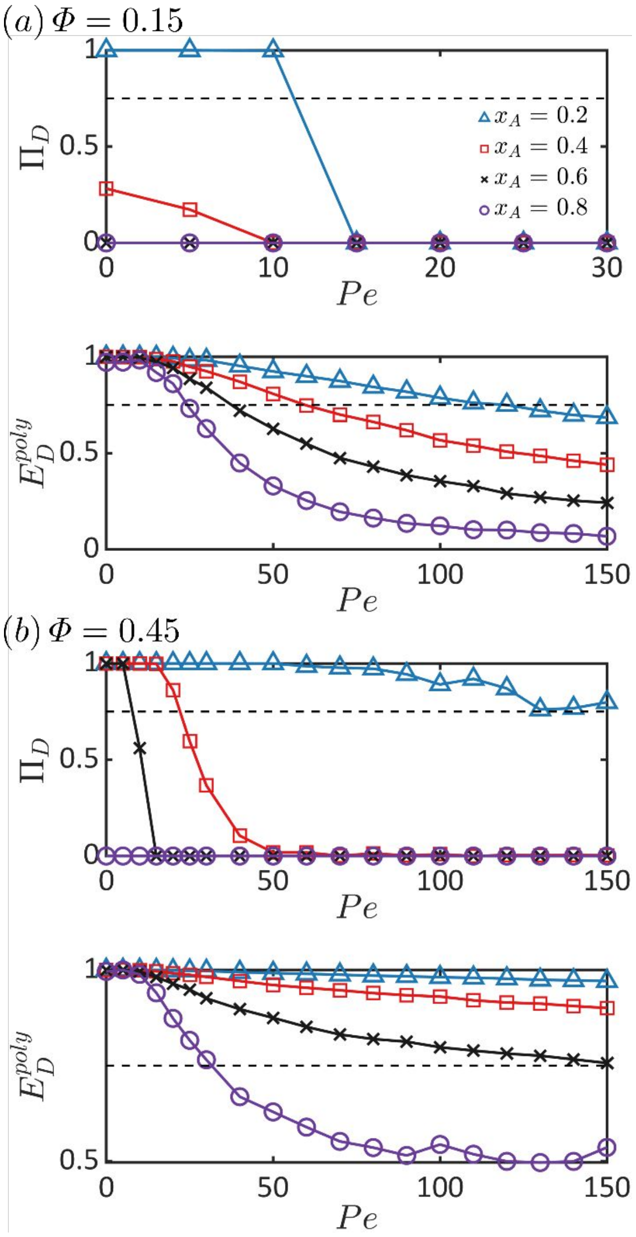

Figure 2: Percolation probability, Π_D, (top) and extent of polymerization, E_D^{poly}, (bottom) versus Péclet number for (a) $\Phi = 0.15$ and (b) $\Phi = 0.45$ and active fractions $x_A = 0.2$ (blue triangles), $x_A = 0.4$ (red squares), $x_A = 0.6$ (black 'x'), and $x_A = 0.8$ (purple circles). The dashed black line in each figure marks where $\Pi_D = 0.75$ or $E_D^{poly} = 0.75$. Results that lies above this line indicate that the system is percolated or polymerized respectively.

Finally, we see that the fraction of active particles in the largest active particle cluster, $\langle n_A^{lc}\rangle/N_A$, increases slightly as Pe increases but is near zero for all Péclet numbers simulated. Figure 1(b) shows these results for the system at area fraction $\Phi = 0.15$ and active particle fraction $x_A = 0.8$. In this figure we see the values of $\langle n_D^{lc}\rangle/N_D$ at $x_A = 0.8$ are much smaller than they were at $x_A = 0.4$, which indicates that much less clustering occurs in these systems. We can see that as Péclet number increases from $Pe = 0$ to $Pe = 10$ the value $\langle n_D^{lc}\rangle/N_D$ increases, but decreases when the Péclet number increases above $Pe = 10$. This follows the same general trend seen for dipolar particles at $x_A = 0.4$ in Figure 1(a). The behavior $\langle n_{All}^{lc}\rangle/N$ mirrors the behavior of $\langle n_D^{lc}\rangle/N_D$ up until $Pe = 60$. Unlike the largest dipolar cluster, the largest cluster of all particles begins to increase slowly when the Péclet number increases above $Pe = 60$. Finally, Figure 1(b) shows that $\langle n_A^{lc}\rangle/N_A$ increases as Pe increases but, as in Figure 1(a), remains small. The small increase in $\langle n_A^{lc}\rangle/N_A$ in both Figure 1(a) and (b) corresponds to the dynamical finite-sized clustering of ABPs at low densities reported elsewhere.[11,39,54] The results for low area fraction mixtures shown in Figure 1(a) and (b) suggest that (1) at low Péclet number, clustering is primarily done by dipolar colloids, (2) slow moving active particles aid in the formation of dipolar colloidal clusters as seen in the initial increase of $\langle n_D^{lc}\rangle/N_D$ at low Pe, and (3) fast

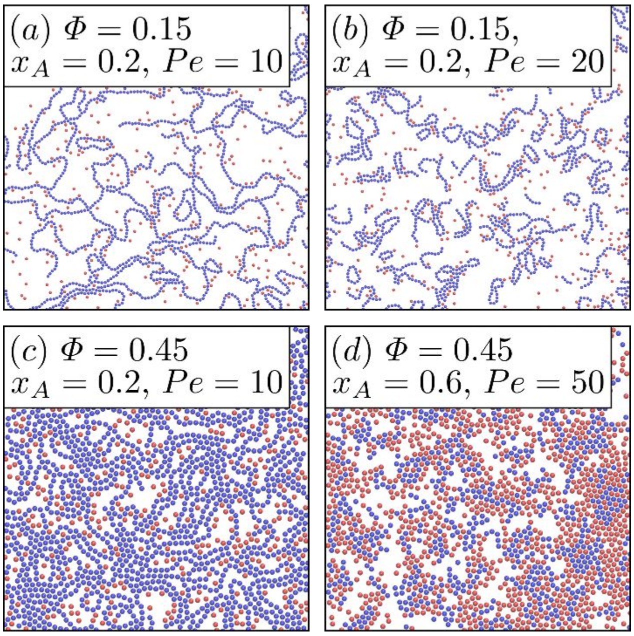

Figure 3: Representative simulation snapshots. (a) Dipolar percolated network at $\Phi = 0.15$, $x_A = 20$, and $Pe = 10$. (b) Dipolar string-fluid at at $\Phi = 0.15$, $x_A = 20$, and $Pe = 20$. (c) Dipolar percolated network at at $\Phi = 0.45$, $x_A = 20$, and $Pe = 10$. (d) Dipolar string-fluid at at $\Phi = 0.45$, $x_A = 60$, and $Pe = 50$. Dipolar particles are blue and active particles are red.

moving active particles disrupt the formation of dipolar colloidal clusters.

Figures 1(c) and (d) show the fraction of particles in the largest cluster for mixtures at area fraction $\Phi = 0.45$ and active particle fraction $x_A = 0.4$ and $x_A = 0.8$, respectively. For Figure 1(c), $\langle n_D^{lc} \rangle / N_D$ is a monotonically decreasing function with increasing Péclet number. This contrasts with the low area fraction systems, where the largest dipolar cluster increases for small Péclet number values above $Pe = 0$. For the active particles in this system, Figure 1(c) shows that $\langle n_A^{lc} \rangle / N_A$ is small for all values up to $Pe \approx 120$, above which $\langle n_A^{lc} \rangle / N_A$ begins to rise. The behavior of the fraction of particles in the largest cluster of all particles, $\langle n_{All}^{lc} \rangle / N$, is more complex. At low Péclet number, $\langle n_{All}^{lc} \rangle / N$ increases as Pe increases until $Pe = 15$. Since at low Pe all the dipolar colloids are already incorporated into a single cluster $\left(\langle n_D^{lc} \rangle / N_D = 1 \right)$, this increase in $\langle n_{All}^{lc} \rangle / N$ can be attributed to active particles colliding with the large dipolar cluster. Above $Pe = 15$, $\langle n_{All}^{lc} \rangle / N$ decreases as the active particles begin to break apart the dipolar cluster. This continues until $Pe = 40$, after which $\langle n_{All}^{lc} \rangle / N$ begins to rise again. This increase is noteworthy because there isn't a significant increase in $\langle n_D^{lc} \rangle / N_D$ or $\langle n_A^{lc} \rangle / N_A$; the likely explanation is that the active and dipolar particles are forming a mixed cluster without any large domain containing one type of particle. In Figure 1(d), once again $\langle n_D^{lc} \rangle / N_D$ is a monotonically decreasing function with increasing Péclet number. For active particles in this system, we see a sharp increase in $\langle n_A^{lc} \rangle / N_A$ at $Pe = 70$ that is characteristic of motility-induced phase separation. The behavior of $\langle n_{All}^{lc} \rangle / N$ mirrors that of the dipolar particle largest cluster fraction at low values of Pe, and that of the active particle largest cluster fraction at high values of Pe. The results for intermediate area fraction mixtures shown in Figure 1(c) and (d) suggest that (1) at low Péclet number, clustering is primarily done by dipolar colloids as was the case for low area fraction mixtures, (2) at low x_A and high Péclet number, large mixed clusters form that contain both types of particles, and (3) at high x_A and high Péclet number, a large active particle cluster forms.

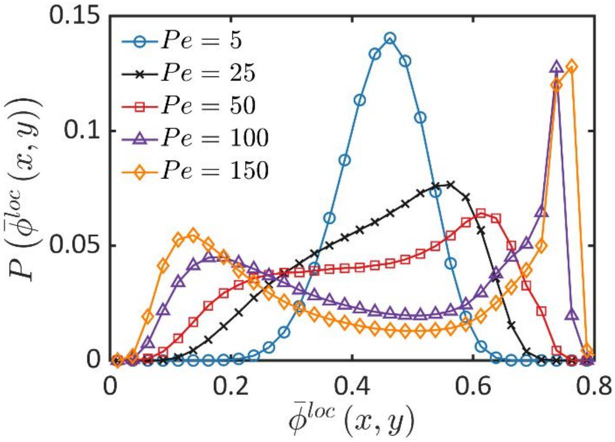

Figure 4: Probability distribtuion of the time-average local area fraction $P\left(\bar{\phi}^{loc}(x,y)\right)$ versus time-average local area fraction $\bar{\phi}^{loc}(x,y)$ for $\Phi = 0.45$, $x_A = 0.8$, and $Pe = 5$ (blue circles), $Pe = 25$ (black 'x'), $Pe = 50$ (red squares), $Pe = 100$ (purple triangles) and $Pe = 150$ (orange diamonds). Lines are drawn between points to help guide the eye.

At low Péclet number for both the low and intermediate density systems, the clusters that form consist primarily of dipolar particles. To further quantify this behavior, we plot the percolation probability, Π_D, and extent of polymerization, E_D^{poly}, versus Péclet number, Pe, for area fractions $\Phi = 0.15$ and $\Phi = 0.45$ in Figure 2(a) and (b), respectively. The percolation probability in the top panel of Figure 2(a) shows that $\Pi_D = 1$ for $x_A = 0.2$ and $Pe = 0, 5, 10$. This indicates that these are the only systems that meet our criteria for the dipolar percolation phase at $\Phi = 0.15$. In addition, Figure 2(a) shows small but non-zero values of Π_D for the systems at $x_A = 0.4$ and $Pe = 0, 5$. These two points represent the same systems for which $\langle n_D^{lc} \rangle / N_D \approx 0.6$ in Figure 1(a). Taken together, this indicates that the large dipolar clusters that form at low area fractions consist of long chains of head-to-tail aligned dipolar colloids as opposed to a compact cluster of these particles. An example of this dipolar network can be seen in the snapshot in Figure 3(a). The extent of polymerization for area fractions $\Phi = 0.15$ in the bottom panel of Figure 2(a) shows that increasing the Péclet number of the active colloids decreases the number of dipolar colloids in clusters, which is in agreement with the trends seen in $\langle n_D^{lc} \rangle / N_D$. This can be seen by comparing the snapshots in Figure 3(a) and (b). These two snapshots represent similar systems, but in Figure 3(a) $(Pe = 10)$ a large dipolar network forms, while in Figure 3(b) $(Pe = 20)$ a dipolar string-fluid forms where the dipolar colloids have assembled into small clusters, short chains, and rings. Additionally, the extent of polymerization, E_D^{poly}, shows a rapid decrease for $x_A = 0.8$ with increasing Péclet number, but this decay is less pronounced as the fraction of active particles, x_A, in the system is reduced. This behavior suggests that the active particles in the mixtures have a similar effect on dipolar

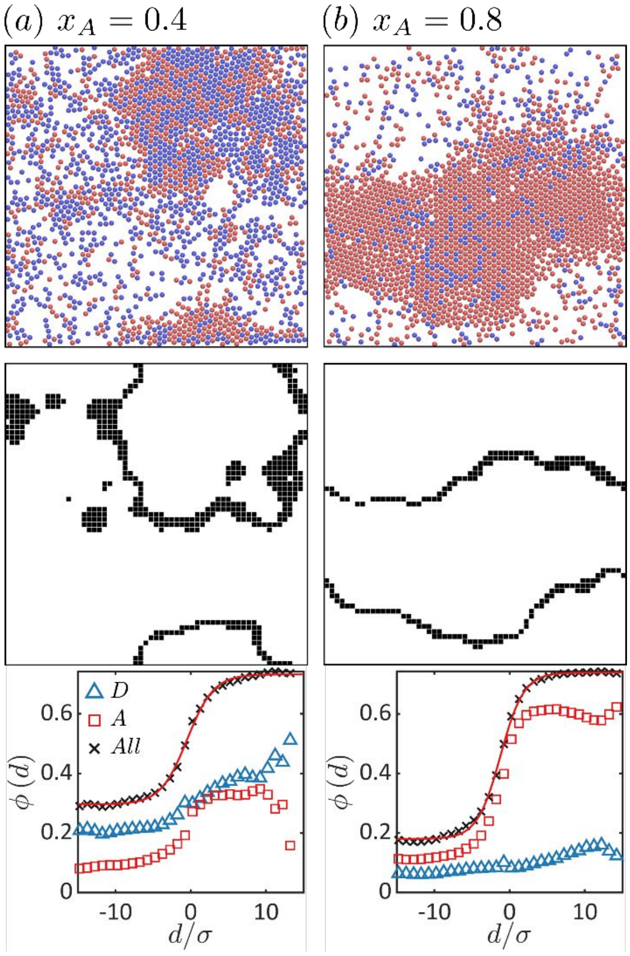

Figure 5: Examples of phase separated systems and interface boundary analysis for $\Phi = 0.45$, $Pe = 150$, and for (a) $x_A = 0.4$ and (b) $x_A = 0.8$. The top image shows a simulation snapshot for these systems. Dipolar colloids are blue and active particles are red. The middle image shows the interfacial boundary (black squares) between the dense and gas phase for these snapshots. The bottom image shows the plot of local area fraction $\phi(d)$ versus distance from the boundary d/σ for dipolar colloids (blue triangles), active colloids (red squares), and all colloids (black 'x'). The red line is the curve fitted by equation 7 with (a) $\phi_{dense} = 0.7329$, $\phi_{gas} = 0.2958$, $d_o = -0.4825$, and $w = 3.5459$ and (b) $\phi_{dense} = 0.7390$, $\phi_{gas} = 0.1797$, $d_o = -1.2204$, and $w = 3.1011$.

clustering as temperature does on pure systems of passive dipolar particles. Both increasing x_A and increasing the Péclet number can be viewed as analogous to increasing the temperature in a passive dipolar system.[79,106] A similar effect can be seen in simulations of active dipolar particles, where increasing particle velocity results in reduced chaining of the active dipolar colloids.[53] For the system at $\Phi = 0.45$ shown in Figure 2(b), the values of both Π_D and E_D^{poly} are larger than those for $\Phi = 0.15$. Indeed, $\Pi_D > 0.75$ for all values of Pe simulated for the systems at $x_A = 0.2$, and even when $x_A = 0.6$ some systems exhibit dipolar percolation. The snapshot in Figure 3(c) shows an example of a percolated system at $\Phi = 0.45$, while Figure 3(d) shows an example of a dipolar-string fluid.

3.2 Phase separation

As we noted earlier, systems at high area fraction exhibit a sharp increase in the largest cluster size of active particles when the Péclet number is high. This behavior is characteristic of motility-induced phase separation, but $\langle n_A^{lc}\rangle/N_A$ alone does not fully describe MIPS. To determine the onset of phase separation, we plot the probability distribution of the time average local area fraction $P(\overline{\phi}^{loc}(x,y))$ at $\Phi = 0.45$ and $x_A = 0.8$ for various values of Pe, an example of which is shown in Figure 4. (We consider both species of colloids regardless of whether they are active or passive in these initial local area fraction calculations; later we will look at what insights can be gained by measuring the local area fractions of dipolar and active colloids independently.) At low Péclet number $(Pe = 5)$, the probability distribution exhibits only one peak, which is centered on the simulation area fraction $\Phi = 0.45$, as would be expected in a homogeneous system. This single peak broadens as the Péclet number increases $(Pe = 25, 50)$. When the Péclet number is $Pe = 100$, two peaks in $P(\overline{\phi}^{loc}(x,y))$ appear, indicating that the mixture phase separates into a dense phase and a dilute phase. The area fractions of particles in these two coexisting phases (ϕ_{dense} for the dense phase and ϕ_{gas} for the dilute phase) correspond to the locations of the two local maxima of $P(\overline{\phi}^{loc}(x,y))$. When $Pe = 150$, the dilute phase peak shifts to a lower value of $\overline{\phi}^{loc}(x,y)$, but the location of the dense phase peak remains unchanged.

To calculate ϕ_{dense} and ϕ_{gas} more exactly, we find the boundary between the dense and dilute phase in the simulation cell, plot the local area fraction versus distance from the boundary, and then fit this data to the Cahn-Hillard ansatz described earlier. Examples of this process are shown in Figure 5 for $\Phi = 0.45$, $Pe = 150$, and $(a)\ x_A = 0.4$ and $(b)\ x_A = 0.8$. In this figure, the top row shows a representative snapshot of the simulation and the middle row shows the corresponding interface between the dense and gas-like phase. The bottom row of Figure 5 shows the plot of local area fraction, $\phi(d)$, versus distance from the boundary, d/σ. In this figure, $d/\sigma < 0$ denotes the dilute region while $d/\sigma > 0$ denotes the dense region. From the fitted line, we can then extract the coexistence area fractions of the dense and dilute phases.

This journal is © The Royal Society of Chemistry 20xx

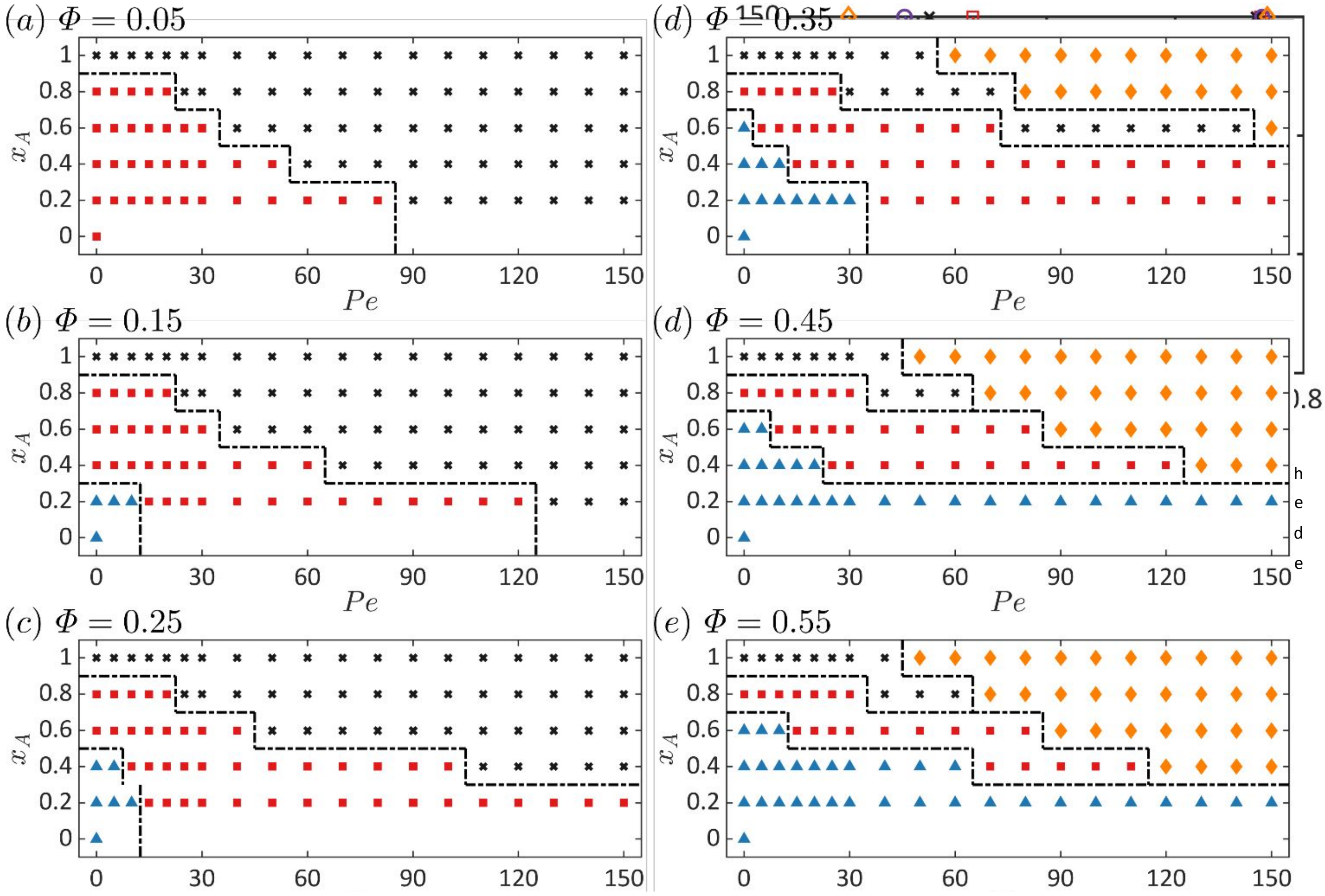

Figure 7: Phase diagrams for constant $\Phi = 0.05 - 0.55$ in the x_A versus Pe plane. The phases exhibited are the percolated dipolar network phase (blue triangles), dipolar string-fluid phase (red squares), isotropic fluid phase (black 'x'), and phase separated state (orange diamonds). Dashed lines are drawn between phases to help guide the eyes.

We plot the coexistence area fractions, ϕ_{dense} and ϕ_{gas}, in the Péclet number versus the local area fraction (Pe,ϕ) plane at various values of x_A and constant system area fraction $\Phi = 0.45$ in Figure 6 to show how the presence of dipolar particles influences these coexistence area fractions. In the limiting case of $x_A = 1$, our data agrees well with previously published results for the low-area fraction branch ϕ_{gas} over the range of Péclet numbers considered.[13] The values for ϕ_{dense} in the high-area fraction branch is close to that for hexagonally close-packing (cp) spheres with a diameter equal to the effective hard sphere diameter σ_h of the spheres in our system, that is $\phi_{cp} = \pi\sigma^2\sqrt{3}/(6\sigma_h^2) \approx 0.72$.[107] The coexistence area fraction of the dilute phase, ϕ_{gas}, shifts towards higher area fractions for each successive decrease in x_A. This may be attributed to the dipolar particles forming clusters in the gas-like phase as can be seen for the low x_A system in the top image in Figure 5(a). In the middle image of Figure 5(a), a few of the small clusters in the gas-like phase have been denoted as part of the interface between the two phases, despite these clusters not lying on the contiguous boundary. Since the interface was obtained by averaging over $\Delta\tau = 0.5\tau$, the presence of these "boundary" areas in the dilute phase indicates that some of the clusters formed in the gas-like phase are long lasting, which would contribute to higher values of ϕ_{gas}. These clusters are largely absent in the high x_A system in Figure 5(b), resulting in lower values of ϕ_{gas}.

We can gain more insight into the distribution of active and dipolar particles in the dense and dilute phases by further examining the local area fraction of the two species independently. To do this, we preform separate Voronoi tessellations on each component of the mixture independently to obtain a local area fraction for dipolar particles, ϕ_D and a local area fraction for active particles ϕ_A. We plot the local area fractions $\phi_D(d)$ and $\phi_A(d)$ versus d/σ in the bottom images of Figure 5(a) and (b), where we are measuring d in relation to the same interface boundary found by considering both species. Here we see that the local area fraction of both species is low in the dilute phase (where $d/\sigma < 0$). As we approach the interface at $d/\sigma = 0$ from the dilute regime, we see that $\phi_A(d)$ begins to rise rapidly and reaches a plateau near $d/\sigma \approx 2.5$. On the other hand, $\phi_D(d)$ increases more gradually than $\phi_A(d)$ in the dilute regime. Taken together, this leads us to conclude that the interfacial layer is rich in active particles. When d/σ is high, both $\phi_D(d)$ and $\phi_A(d)$ begin to fluctuate, indicating small single component domains within the dense phase.

3.3 Phase diagrams

Combining all this information, we plot the phase diagrams for $\Phi = 0.05, 0.15, 0.25, 0.35, 0.45,$ and 0.55 in the x_A versus Pe plane shown in Figure 7(a)-(e), respectively. Starting with

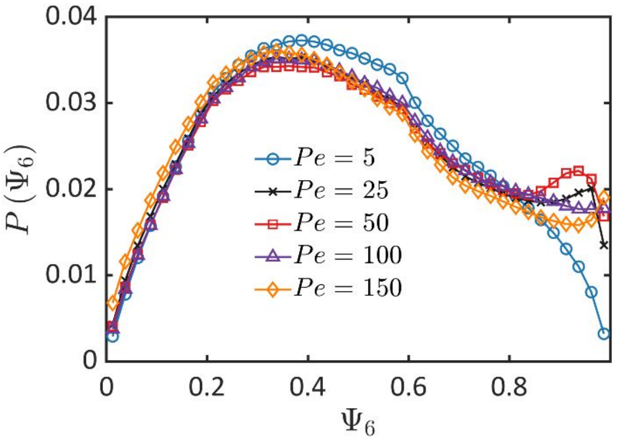

Figure 8: Probability distribution of the hexagonal bond-orientational order parameter, $P(\Psi_6)$, for $\Phi = 0.55$, $x_A = 0.2$, and $Pe = 5$ (blue circles), $Pe = 25$ (black 'x'), $Pe = 50$ (red squares), $Pe = 100$ (purple triangles) and $Pe = 150$ (orange diamonds). Lines are drawn between points to help guide the eye.

$\Phi = 0.05$, the system is not dense enough to form a percolated network, and the only phases present are the string-fluid and isotropic fluid phases. This agrees with results from simulations of two-dimensional dipole-like colloids which show that low density systems will not percolate.[79] At $\Phi = 0.15$ the percolated dipolar network phase forms at low Péclet number, and $x_A = 0$ and 0.2, while the rest of the phase diagram closely matches that at $\Phi = 0.05$. The results at $x_A = 0$ agree with previous simulations which show that at low temperatures a pure system of dipolar particles will percolate above $\Phi \approx 0.10$.[79] At $\Phi = 0.25$, the percolated network now forms at $x_A = 0.4$, and the string-fluid phase persists at higher values of Pe. At $\Phi = 0.35$, this trend continues, with the percolated network and string-fluid persisting at higher Pe. In addition, we begin to see the two-phase state at high Pe when x_A is high. At $\Phi = 0.45$, the two-phase region begins to form at lower Pe and x_A. Finally, at $\Phi = 0.55$, the percolated network phase persists when $x_A = 0.2$ for all values of Pe considered in this study, although at high Péclet number this percolated network consists of large domains of hexagonal close packed dipolar discs instead of the head-to-tail aligned chains found at lower values of Pe. This can be seen in Figure 8, which shows the probability distribution of the hexagonal bond-orientational order parameter $P(\Psi_6)$. From this figure we can see the development of a peak near $\Psi_6 = 1$ as the Péclet number increases, but this peak is absent at low values of Pe.

We did not find any Péclet number at which very low x_A systems form a two-phase state. This contrasts with what has been seen in simulations of active and passive repulsive discs, in which systems with as little as 15% active particles can phase separate.[66] However we did not investigate the behavior at very high Péclet number $(Pe \approx 500)$ where this behavior has been found. There are two possible results that could be seen at very high Péclet number. The first possibility is that phase separation in the dipolar and active mixture at low x_A would require a lower Péclet number to achieve phase separation than is found in the passive/active mixture because the dipolar interactions would act as a stabilizing force to keep clustered dipolar particles together. This has been checked by running two brief simulations (data not shown) starting from the last configuration of the $\Phi = 0.55$, $x_A = 0.2$, $Pe = 150$, and dipolar coupling strength $\lambda = 10$ system. In the first simulation we set the dipolar coupling strength as $\lambda = 10$ and the Péclet number as $Pe = 0$ and observe that the structure undergoes very little rearrangement, largely maintaining the shape found in the initial configuration. In the second simulation we set the dipolar coupling strength as $\lambda = 0$ and the Péclet number as $Pe = 0$ and observe that the particles quickly disperse into a homogenous, isotropic fluid. The second possibility is that phase separation in the dipolar and active mixture at low x_A would require a higher Péclet number to achieve phase separation, or indeed phase separation may not be possible at low x_A. Investigations into strongly coupled equilibrium dipolar fluids[79] and active dipolar fluids[53] show that strongly coupled dipolar particles prefer forming head-to-tail aligned chains and resist phase separation.

Conclusions

We have calculated phase diagrams for mixtures of dipolar spheres and active spheres using Brownian dynamics. These mixtures form percolated dipolar networks, string-fluids, isotropic fluids, or phase separate into a dense and dilute phase based on the system parameters. When the motility of the active particles is small, as measured by the Péclet number, the dipolar particles form rings or short chains at low area fractions, and long chains or percolated networks at high area fractions. When the motility of the active particles is increased, the long chains of dipolar particles are disrupted and are either broken apart into short chains or pushed into denser clusters. These short dipolar chains arise when the number of active particles is large, or when the area fraction of the system is low. Large area fractions with low numbers of active particles result in dense clusters of dipolar chains. When the motility of the active particles reaches a certain threshold and the area fraction is sufficiently high, the system undergoes motility-induced phase separation.

This work builds upon previous simulation and theoretical results for mixtures of colloidal particles. Much of focus has been on mixtures that interact via isotropic steric repulsion forces only.[33,66-71] However some work has been done that has considered particles that interact via anisotropic steric repulsion[32] or polar velocity alignment.[34] These previous papers have focused on phase separation and demixing behavior. By simulating mixtures that contain passive dipolar colloids, we have introduced particles with an anisotropic interaction that can be either attractive or repulsive in nature, in addition to the steric repulsion forces. This additional interaction leads to enhanced clustering and chain formation at lower Péclet numbers compared to the clustering that occurs in the active/passive mixtures that have previously been studied.

The phase diagrams calculated in this work can aid experimentalists in understanding the complex aggregation behavior seen in colloidal mixtures. In particular, the mixture of dipolar colloids and active colloids shows an interplay between the two species of particles. The dipolar colloids prefer to form head-to-tail aligned chains, and the active particles either break up the chains of dipolar particles or phase separate, causing the dipolar particles to adopt a hexagonal, close-packed structure. These mixtures could be useful in creating novel materials that can adopt different configurations by adjusting the motility of the active particles.

We have investigated systems with a high dipolar coupling strength λ so that the attractive dipolar interactions are sufficiently strong compared to the repulsive interactions induced by fast moving active particles. We predict that a lower dipolar coupling strength would cause dipolar clusters to break apart at lower active particle Péclet number. When the coupling strength is sufficiently low, these mixtures would exhibit little dipolar clustering and instead behave like the mixtures of active and passive particles that have been investigated by others.[66,68]The relative strength of interactions between the passive particles could be determined by monitoring the breaking of chains of passive particles as the active particle Péclet number increases, as stronger interacting particles would exhibit chaining and clustering at higher Péclet number than weaker interacting particles would. It would also be of interest to consider active/passive mixtures in which the passive particles exhibit other types of interactions, such as Lennard-Jones interactions. Since Lennard-Jones interactions do not depend on the orientation of the particles and do not prefer head-to-tail configurations, it is likely that these passive particles would form denser clusters that remain intact at higher active particle Péclet number. Knowledge of this could lead to the development of a tool that could predict passive particle interactions when these interactions are not know a priori.

One intriguing area for future study of these mixtures would be to introduce an isotropic attractive force between the dipolar colloids, such as the capillary force that is present in lipid coated magnetic nanoparticles studied by Bharti et al.[108] The capillary force in their system was estimated to be ≈ 25 times stronger than the magnetic force, which would serve to keep the dipolar particles in clusters even in the presence of high Péclet number active particles. Colloidal particles that combine the strong capillary force with orientation-dependent dipolar interactions could lead to interesting interactions between these particles and active colloids. A second area of future research would be to see if active colloids can be used to induce long range ferromagnetic clusters in the passive dipolar particles. This may be possible by introducing another source of anisotropy, such as rod-shaped dipolar particles or circular swimming active particles, both of which could encourage separation between the two species. Finally, we could extend this work by considering how hydrodynamic and phoretic forces impact the active/dipole mixtures. The effects of these forces are difficult to predict but could lead to demixing of the active and dipolar particles or promoting long range ferromagnetic order among the dipolar particles.

Conflicts of interest

There are no conflicts to declare.

Acknowledgements

This work was supported by NSF's Research Triangle MRSEC under grant number DMR-1121107, and by OISE-1065466. It was also supported by the German Research Foundation (DFG) through grant IRTG 1524. We would also like to thank Drs. David Rutkowski and Orlin Velev for helpful discussions.

Notes and references

1 F. Schweitzer, *Brownian Agents and Active Particles: Collective Dynamics in the Natural and Social Sciences*, Springer, Berlin, 2003.
2 P. Romanczuk, M. Bär, W. Ebeling, B. Lindner and L. Schimansky-Geier, Eur. *Phys. J.-Spec. Top.*, 2012, **202**, 1.
3 C. Dombrowski, L. Cisneros, S. Chatkaew, R. E. Goldstein and J. O. Kessler, *Phys. Rev. Lett.*, 2004, **93**, 098103.
4 A. E. Patteson, A. Gopinath and P. E. Arratia, *Nat. Commun.*, 2018, **9**, 5373.
5 A. Cavagna, A. Cimarelli, I. Giardina, A. Orlandi, G. Parisi, A. Procaccini, R. Santagati and F. Stefanini, *Math. Biosci.*, 2008, **214**, 32-37.
6 A. Cavagna, A. Cimarelli, I. Giardina, G. Parisi, R. Santagati, F. Stefanini and M. Viale, *Proc. Natl. Acad. Sci. U. S. A.*, 2010, **107**, 11865.
7 C. Becco, N. Vandewalle, J. Delcourt and P. Poncin, *Physica A*, 2006, **367**, 487.
8 D. Helbing and P. Molnar, Phys. Rev. E, 1995, **51**, 4282.
9 Y. Jiang, B. Chen, B. Wang, W. Wong and B. Cao, Front. *Phys.-Beijing*, 2017, **12**, 124502.
10 Z. Kang, L. Zhang and K. Li, *Appl. Math. Comput.*, 2019, **348**, 355.
11 I. Theurkauff, C. Cottin-Bizonne, J. Palacci, C. Ybert and L. Bocquet, *Phys. Rev. Lett.*, 2012, **108**, 268303.
12 M. E. Cates and J. Tailleur, *EPL*, 2013, **101**, 20010.
13 J. Bialké, T. Speck and H. Löwen, *J. Non-Cryst. Solids*, 2015, **407**, 367.
14 H. H. Wensink, J. Dunkel, S. Heidenreich, K. Drescher, R. E. Goldstein, H. Löwen and J. M. Yeomans, *Proc. Natl. Acad. Sci. U. S. A.*, 2012, **109**, 14308.
15 S. Heidenreich, J. Dunkel, S. H. L. Klapp and M. Bär, *Phys. Rev. E*, 2016, **94**, 020601.
16 Reinken, S. H. L. Klapp, M. Bär and S. Heidenreich, *Phys. Rev. E*, 2018, **97**, 022613.
17 Vicsek, A. Czirók, E. Ben-Jacob, I. Cohen and O. Shochet, *Phys. Rev. Lett.*, 1995, **75**, 1226.
18 J. Buhl, D. Sumpter, I. D. Couzin, J. J. Hale, E. Despland, E. R. Miller and S. J. Simpson, *Science, 2006*, **312**, 1402.
19 H. P. Zhang, A. Be'er, R. S. Smith, E.-L. Florin and H. L. Swinney, *EPL*, 2009, **87**, 48011.
20 M. F. Copeland and D. B. Weibel, *Soft Matter*, 2009, **5**, 1174.
21 A. Kudrolli, G. Lumay, D. Volfson and L. S. Tsimring, *Phys. Rev. Lett.*, 2008, **100**, 058001.
22 F. Kogler, O. D. Velev, C. K. Hall and S. H. L. Klapp, *Soft Matter*, 2015, **11**, 7356.
23 C. W. Waechtler, F. Kogler and S. H. L. Klapp, *Phys. Rev. E*, 2016, **94**, 052603.
24 R. Dreyfus, J. Baudry, M. L. Roper, M. Fermigier, H. A. Stone and J. Bibette, *Nature*, 2005, **437**, 862.

25 J. R. Howse, R. A. L. Jones, A. J. Ryan, T. Gough, R. Vafabakhsh and R. Golestanian, *Phys. Rev. Lett.*, 2007, **99**, 048102.
26 A. Erbe, M. Zientara, L. Baraban, C. Kreidler and P. Leiderer, *J. Phys.-Condens. Mat.*, 2008, **20**, 404215.
27 J. Palacci, C. Cottin-Bizonne, C. Ybert and L. Bocquet, *Phys. Rev. Lett.*, 2010, **105**, 088304.
28 G. Volpe, I. Buttinoni, D. Vogt, H. Kuemmerer and C. Bechinger, *Soft Matter*, 2011, **7**, 8810.
29 L. Baraban, D. Makarov, R. Streubel, I. Moench, D. Grimm, S. Sanchez and O. G. Schmidt, *Acs Nano*, 2012, **6**, 3383.
30 D. A. Wilson, R. J. M. Nolte and van Hest, Jan C. M., *Nat. Chem.*, 2012, **4**, 268.
31 J. Palacci, S. Sacanna, A. P. Steinberg, D. J. Pine and P. M. Chaikin, *Science*, 2013, **339**, 936.
32 S. R. McCandlish, A. Baskaran and M. F. Hagan, *Soft Matter*, 2012, **8**, 2527.
33 Z. Ma, Q. Lei and R. Ni, *Soft Matter*, 2017, **13**, 8940.
34 B. Ai, Z. Shao and W. Zhong, *Soft Matter*, 2018, **14**, 4388.
35 R. Ni, M. A. C. Stuart, M. Dijkstra and P. G. Bolhuis, *Soft Matter*, 2014.
36 S. K. Das, S. A. Egorov, B. Trefz, P. Virnau and K. Binder, *Phys. Rev. Lett.*, 2014, **112**, 198301.
37 J. Elgeti, R. G. Winkler and G. Gompper, *Rep. Prog. Phys.*, 2015, **78**, 056601.
38 M. C. Marchetti, Y. Fily, S. Henkes, A. Patch and D. Yllanes, *Curr. Opin. Colloid In.*, 2016, **21**, 34.
39 I. Buttinoni, J. Bialké, F. Kümmel, H. Löwen, C. Bechinger and T. Speck, *Phys. Rev. Lett.*, 2013, **110**, 238301.
40 J. Tailleur and M. E. Cates, *Phys. Rev. Lett.*, 2008, **100**, 218103.
41 P. Digregorio, D. Levis, A. Suma, L. F. Cugliandolo, G. Gonnella and I. Pagonabarraga, *Phys. Rev. Lett.*, 2018, **121**, 098003.
42 G. S. Redner, C. G. Wagner, A. Baskaran and M. F. Hagan, *Phys. Rev. Lett.*, 2016, **117**, 148002.
43 G. S. Redner, M. F. Hagan and A. Baskaran, *Phys. Rev. Lett.*, 2013, **110**, 055701.
44 J. Stenhammar, A. Tiribocchi, R. J. Allen, D. Marenduzzo and M. E. Cates, *Phys. Rev. Lett.*, 2013, **111**, 145702.
45 C. Nardini, É Fodor, E. Tjhung, F. van Wijland, J. Tailleur and M. E. Cates, *Phys. Rev. X*, 2017, **7**, 021007.
46 A. Baskaran and M. C. Marchetti, *Phys. Rev. E*, 2008, **77**, 011920.
47 A. Baskaran and M. C. Marchetti, *Phys. Rev. Lett.*, 2008, **101**, 268101.
48 J. Blaschke, M. Maurer, K. Menon, A. Zöttl and H. Stark, *Soft Matter*, 2016, **12**, 9821.
49 N. Yoshinaga and T. B. Liverpool, *Phys. Rev. E*, 2017, **96**, 020603.
50 F. J. Schwarzendahl and M. G. Mazza, *J. Chem. Phys.*, 2019, **150**, 184902.
51 E. Mani and H. Löwen, *Phys. Rev. E*, 2015, **92**, 032301.
52 M. Pu, H. Jiang and Z. Hou, *Soft Matter*, 2017, **13**, 4112.
53 G. Liao, C. K. Hall and S. H. L. Klapp, *Soft Matter, 2020, **16**, 2208*.
54 G. Liao and S. H. L. Klapp, *Soft Matter*, 2018, **14**, 7873.
55 Y. Peng, L. Lai, Y. Tai, K. Zhang, X. Xu and X. Cheng, *Phys. Rev. Lett.*, 2016, **116**, 068303.
56 A. Das, A. Polley and M. Rao, *Phys. Rev. Lett.*, 2016, **116**, 068306.
57 N. A. Mecholsky, E. Ott and T. M. Antonsen Jr., *Physica D*, 2010, **239**, 988.
58 A. Sengupta, T. Kruppa and H. Löwen, *Phys. Rev. E*, 2011, **83**, 031914.
59 K. C. Leptos, J. S. Guasto, J. P. Gollub, A. I. Pesci and R. E. Goldstein, *Phys. Rev. Lett.*, 2009, **103**, 198103.
60 J. Dunkel, V. B. Putz, I. M. Zaid and J. M. Yeomans, *Soft Matter*, 2010, **6**, 4268.
61 G. L. Mino, J. Dunstan, A. Rousselet, E. Clement and R. Soto, *J. Fluid Mech.*, 2013, **729**, 423.
62 A. Jepson, V. A. Martinez, J. Schwarz-Linek, A. Morozov and W. C. K. Poon, *Phys. Rev. E*, 2013, **88**, 041002.
63 A. Brown and W. C. K. Poon, *Soft Matter*, 2014, **10**, 4016.
64 S. Ramananarivo, E. Ducrot, and J Palacci, *Nat. Commun., 2019, **10***, 3380.
65 J. Harder, S. A. Mallory, C. Tung, C. Valeriani, and A. Cacciuto, *J. Chem. Phys.*, 2014, **141**, 194901.
66 J. Stenhammar, R. Wittkowski, D. Marenduzzo and M. E. Cates, *Phys. Rev. Lett.*, 2015, **114**, 018301.
67 A. Wysocki, R. G. Winkler and G. Gompper, *New J. Phys.*, 2016, **18**, 123030.
68 R. Wittkowski, J. Stenhammar and M. E. Cates, *New J. Phys.*, 2017, **19**, 105003.
69 P. Dolai, A. Simha and S. Mishra, *Soft Matter*, 2018, **14**, 6137.
70 F. Alaimo and A. Voigt, *Phys. Rev. E*, 2018, **98**, 032605.
71 G. Pessot, H. Löwen and A. M. Menzel, *Mol. Phys.*, 2018, **116**, 3401.
72 B. van der Zande, G. Koper and H. Lekkerkerker, *J. Phys Chem B*, 1999, **103**, 5754.
73 K. D. Hermanson, S. O. Lumsdon, J. P. Williams, E. W. Kaler and O. D. Velev, *Science*, 2001, **294**, 1082.
74 S. Gangwal, O. J. Cayre and O. D. Velev, *Langmuir*, 2008, **24**, 13312
75 S. K. Smoukov, S. Gangwal, M. Marquez and O. D. Velev, *Soft Matter*, 2009, **5**, 1285.
76 K. Han, C. W. Shields and O. D. Velev, *Adv. Funct. Mater.*, 2018, **28**, 1705953.
77 T. C. Halsey and W. Toor, *Phys. Rev. Lett.*, 1990, **65**, 2820.
78 A. Goyal, C. K. Hall and O. D. Velev, *Physical Review E*, 2008, **77**, 031401.
79 H. Schmidle, C. K. Hall, O. D. Velev and S. H. L. Klapp, *Soft Matter*, 2012, **8**, 1521.
80 A. Kaiser, K. Popowa and H. Löwen, *Physical Review E*, 2015, **92**, 012301.
81 F. Guzman-Lastra, A. Kaiser and H. Löwen, *Nat. Commun.*, 2016, **7**, 13519.
82 A. Kaiser, A. Snezhko and I. S. Aranson, *Sci. Adv.*, 2017, **3**, e1601469.
83 G. Kokot and A. Snezhko, *Nat. Commun.*, 2018, **9**, 2344.
84 R. P. Blakemore, *Annu. Rev. Microbiol.*, 1982, **36**, 217.
85 R. B. Frankel, *Annu. Rev. Biophys. Bioeng.*, 1984, **13**, 85.
86 N. Waisbord, C. T. Lefèvre, L. Bocquet, C. Ybert and C. Cottin-Bizonne, *Phys. Rev. Fluids*, 2016, **1,** 053203.
87 S. Klumpp, C. T. Lefevre, M. Bennet and D. Faivre, *Phy. Rep.*, 2019, **789**, 1.
88 P. Langevin, *C. R. Hebd. Séances Acad. Sci.*, 1908, **146**, 530.
89 D. S. Lemons and A. Gythiel, *Am. J. Phys.*, 1997, **65**, 1079.
90 J. D. Weeks, D. Chandler and H. C. Andersen, *J. Chem. Phys.*, 1971, **54**, 523.
91 E. Madelung, *Phys. Z.*, 1918, **19**, 524.
92 P. P. Ewald, Ann. *Phys.-Berlin*, 1921, **64**, 253.
93 J. W. Perram and S. W. de Leeuw, *Physica A*, 1981, **109**, 237.
94 . R. Smith, *Mol. Phys.*, 1982, **45**, 915.
95 E. Spohr, *J. Chem. Phys.*, 1997, **107**, 6342.
96 J. A. Barker and D. Henderson, *J. Chem. Phys.*, 1967, **47**, 285.
97 Y. Fily, S. Henkes and M. C. Marchetti, *Soft Matter*, 2014, **10**, 2132.
98 D. Levis, J. Codina and I. Pagonabarraga, *Soft Matter*, 2017, **13**, 8113.
99 A. P. Solon, J. Stenhammar, M. E. Cates, Y. Kafri and J. Tailleur, *Phys. Rev. E*, 2018, **97**, 020602.
100 I. R. Bruss and S. C. Glotzer, *Phys. Rev. E*, 2018, **97**, 042609.

Please do not adjust margins

101 Y. Fily and M. C. Marchetti, *Phys. Rev. Lett.*, 2012, **108**, 235702.

102 L. Rovigatti, J. Russo and F. Sciortino, *Soft Matter*, 2012, **8**, 6310.

103 H. Neitsch and S. H. L. Klapp, *J. Chem. Phys.*, 2013, **138**, 064904.

104 J. W. Cahn and J. E. Hilliard, *J. Chem. Phys.*, 1958, **28**, 258.

105 S. Jäger, H. Schmidle and S. H. L. Klapp, *Phys. Rev. E*, 2012, **86**, 011402.

106 S. S. Kantorovich, A. O. Ivanov, L. Rovigatti, J. M. Tavares and F. Sciortino, *Phys. Chem. Chem. Phys.*, 2015, **17**, 16601.

107 H. Chang and L. Wang, *arXiv:1009.4322 [math.MG]*, 2010, 1.

108 B. Bharti, A. Fameau, M. Rubinstein and O. D. Velev, *Nat. Mater.*, 2015, **14**, 110.

This journal is © The Royal Society of Chemistry 20xx

Please do not adjust margins

Mixtures of dipolar and active colloidal particles display a variety of states including chains, string-fluids, and motility induced phase separation.